Applied Radiation and Isotopes 165 (2020) 109303

Contents lists available at ScienceDirect

Applied Radiation and Isotopes

journal homepage: http://www.elsevier.com/locate/apradiso

Classification of radiological objects at the exit of accelerators with a dose-rate constraint

Thomas Frosio *, Gerald Dumont, Robert Froeschl, Elpida Iliopoulou, Matteo Magistris, Nabil Menaa, Stefan Roesler, Chris Theis, Heinz Vincke, Helmut Vincke

Radiation Protection Group, European Organization for Nuclear Research, 1211, Geneva 23, Switzerland

ARTICLE INFO

Keywords:
Radiological waste characterization
Classification
Monte-carlo simulations
ActiWiz
Clearance of material

ABSTRACT

Maintenance activities and operations of high-energy particle accelerators can lead to the collection of radioactive equipment as well as waste materials. In order to ensure their proper classification as radioactive or non-radioactive, one has to quantify the activities of radionuclides produced. According to the regulatory requirements in Switzerland, these activities need to be compared with nuclide-specific clearance limits. In particular, a new set of clearance limits was introduced by the Swiss authorities in January 2018, leading to more conservative values for a number of relevant radionuclides. We describe in this paper a new methodology based on dose-rate measurements to classify potentially radioactive objects at the exit of the CERN accelerator complex. This methodology concerns the specific material compositions typically found at CERN and takes into account the latest clearance limits introduced by the Swiss authorities.

1. Introduction

Since January 2018, new clearance limits (LL) have been introduced in the ORAP (Ordonnance sur la RAdioProtection) (Ordonnance sur la radiopr, 2018) and replace the previous exemption values (LE). One of the major changes is the fact that LL limits for important radionuclides are often considerably more conservative than LE. For example, the LE limit for Co-60 was 1 Bq/g, whereas the LL limit is 0.1 Bq/g. Mn-54 is one of the practically most limiting nuclides in activated metallic components containing iron. The limiting characteristic is explained by the fact that the Mn-54 nuclide is highly produced in activated iron whereas its clearance limit is relatively low since its value changed from 10 Bq/g to 0.1 Bq/g in the newly released regulatory ordinance (Ordonnance sur la radiopr, 2018).

This document presents the calculations performed to determine the possibility of classifying materials according to the new LL limits by an ambient dose equivalent rate measurement and to develop an in-situ radiological classification method (Walter, 2015). The purpose is to ensure regulatory compliance, keep efficiency in materials classification, optimize and reduce the number of extended measurements.

The classification of potentially radioactive waste has always required a considerable number of measurements at CERN. In the near future, large maintenance campaigns are planned at CERN from 2019 to 2020 during the so-called LS2 period (Long-Shutdown 2), leading to a production increase of waste that is to be classified. Based on the first Long-Shutdown LS1, we extrapolated the number of needed measurements to classify material. The forecasted number of measurements can reach around 50 000 during LS2 (2019–2020), while the number of performed measurements reached around 40 000 during the previous Long Shutdown LS1 (2013–2014).

The first section of the documents details the device which will be used for the material classification. The second section presents the calculations performed to reach a classification criterion by ambient dose equivalent rate measurement. The third section consists in a risk analysis and the impact of potential mistakes that might occur during the classification of a material. Finally, an experimental verification is described in the last section which was carried out to demonstrate the applicability of the method.

2. Detection limit of ambient dose equivalent rate measurements

The FHZ 512 BGO [1]is a scintillator-based radiation rate meter that has been used at CERN until today, to identify radioactive objects at the

* Corresponding author.
E-mail address: thomas.frosio@gmail.com (T. Frosio).
[1] https://www.thermofisher.com/order/catalog/product/4254002.

https://doi.org/10.1016/j.apradiso.2020.109303
Received 16 January 2020; Received in revised form 28 May 2020; Accepted 17 June 2020
Available online 6 July 2020

exit from the accelerators. In what follows, we refer to this rate meter simply as BGO. This BGO was extensively studied and tested before its deployment in order to ensure a high level of sensitivity, required for its use in the field (Neff, 2382). It was selected for its higher detection efficiency compared to other scintillation detectors such as NaI, for its resistance to wear and tear in CERN's working environments and its stability under different thermal conditions.

The detection limit ρ_n of the BGO can be calculated with Equation (1) from ISO11929-1 (ISO11929), where $k_{1-\alpha}$ and $k_{1-\beta}$ are the quantiles of the standard normal distribution for the errors of the first and second kind (set to 5% for the present study as usually done (Klumpp et al., 2018)), and t_0 and t_s are the background and sample counting times.

$$\rho_n = (k_{1-\alpha} + k_{1-\beta})\sqrt{\rho_0\left(\frac{1}{t_0}+\frac{1}{t_s}\right)} + \frac{1}{4}(k_{1-\alpha} + k_{1-\beta})^2\left(\frac{1}{t_0}+\frac{1}{t_s}\right) \quad (1)$$

Equation (1). Detection limit as a function of quantiles and counting time.

In all the next of the document, we refer to "dose rate" as ambient dose equivalent rate.

3. A minimum detectable dose rate (MDDR) for material classification

Considering a 60 s counting time and a background rate of 35 count/s, Equation (1) allows detecting signals above 5 nSv/h. Consequently, an MDDR of 5 nSv/h has been chosen for objects classification. In what follows, we will assess whether an object with a dose rate below 5 nSv/h can be classified as non-radioactive with respect to the new LL limits. The goal will be to determine a set of object physical characteristics with LL above 1 and a dose rate below 5 nSv/h. This will allow excluding them in the classification procedure. The remaining sub-set of objects will be guaranteed to be classified as not radioactive when the dose rate values are below 5 nSv/h."The field of application of such MDDR is evaluated by means of a so-called factor analysis. This analysis is based on extensive ActiWiz calculations (section 2.1). The MDDR is then validated with a statistical analysis based on experimental data recorded via TREC (Traceability of Radioactive Equipment at Cern) (Kepinski et al, 2013a). TREC is the official system used at CERN to trace potentially radioactive equipment. It replaces paper work by electronic data, manual phone calls by automatic email notifications and helps to enforce CERN safety rules. Some of the major benefits are the reduction of the delays related to equipment movements (from installation to workshops or waste storage areas) as well as increased personal safety. TREC allows to manage and track all equipment potentially radioactive from measurement request, radiation control to equipment handling.

The parameter of interest for this study is the dose rate at 10 cm distance per unit of clearance limit (nSv/h), which we will refer to as DR/LL. The DR/LL is defined in Equation (2):

$$\frac{DR}{LL} = \frac{DR}{\sum_{i=1}^{n}\frac{A_i}{ll_i}} \quad (2)$$

Equation (2). Dose rate per unit of LL.Where: A_i represents the specific activity of the radionuclide i in the object and ll_i its clearance limit, given in (Ordonnance sur la radiopr, 2018).

The distance is selected at 10 cm so that, the object will be inside the solid angle of the measurement device. This parameter is of interest for the calculations (gamma attenuation follows an exponential law). In the present context, the clearance limit represents the most restrictive value between absolute and specific activities, depending on the properties of the object (cf art 106.b from ORaP (Ordonnance sur la radiopr, 2018)).

3.1. Factor analysis

Factor Analysis of Mixed Data is a principal component method (Wold et al., 1987). It allows to explore data when continuous and categorical variables are considered. It is often used to view the relations between individuals and variables by simplifying the complexity of high dimensions problems. The data dimension is reduced by performing data projection on an eigenvector. The new dimensions are called principal components. The reader can get more information about principal component methods with reference (Jolliffe and Cadima, 2015). In the frame of the FAMD (Pagès, 2014), we first define a set of possible activation scenarios by identifying a list of input parameters (e.g. cooling time) with a range of values (e.g. from 3 h to 2 years). It should be noted that the cooling times were restricted to a maximum of 2 years as the procedure focusses on objects that are removed from the accelerators/experiments within the maximum time frame of a long shutdown. Longer cooling periods have intentionally been omitted to avoid becoming over-restrictive while being aware that this would mean that the generic MDDR cannot be applied to historic waste. The FAMD is performed only in order to perform a qualitative sensitivity analysis of the activation scenario parameters that we need to constraint. The purpose is not here to perform the whole study with big data techniques as the result have to be simple and pragmatic for operational reasons.

We then use ActiWiz 3.3 (Theis and Vincke) to calculate the value of dose rate per radiotoxicity level (DR/LL) for each activation scenario. The DR/LL can also be regarded as the expected dose rate for an object with LL equal 1. Consequently, a value of DR below the DR/LL indicates that an object can be classified as non-radioactive (leading to an LL below 1).

The parameters that influence the radionuclide inventory and the clearance limit of an object are the irradiation and cooling times, the energy of primary particles, the material, and the location in accelerator machine. The radionuclide inventory also influences the dose rate. On the other side, the size of an object has also an impact on the measured dose rate. Using the factor analysis, our objective is to define the physical parameters that need to be constrained in order to ensure a dose rate below 5 nSv/h for LL equal 1. The objective of the factor analysis, using ActiWiz calculations, is to identify suitable constraints of input parameters (e.g. dimensions, irradiation and cooling periods, etc.) in such a way, that they allow for classifying a reasonably large number of items at the exit of accelerators via dose rate measurements. ActiWiz calculations consist in varying the irradiation and cooling times as well as the primary particle energies and object location in accelerators to predict the nuclide inventories and the associated dose rate for the simulated irradiated objects.

The selection of input parameters partition leads to the definition of sorting criteria at the exit from accelerators. Such criteria need to be optimized, in the sense that they shall:

- be of simple application at the exit from the accelerators (e.g., focus on measurable quantities like the size of the object);
- ensure the robustness of the method (i.e., minimize the risk of false negatives: radioactive items which would be classified as non-radioactive because of too relaxed sorting criteria); and
- be reasonably conservative (i.e., minimize the risk of false positive: non-radioactive items which would be classified as radioactive because of too strict sorting criteria).

Over 1.2 million activation scenarios were calculated using a proprietary Python scripting interface to ActiWiz 3.3 (Vincke and Theis, 2018) that had been developed to allow for customized massive calculations. This allowed for a comprehensive study varying radiation fields, object geometries and common materials at CERN in a computationally very efficient way. The complete list of retained input variables and corresponding values ranges is given below:

- Irradiation time from 1 day to 30 years;
- Cooling time from 3 hours to 2 years;
- Dimension of objects, surface from 1 x 1 to 30 x 30 cm^2 and thickness from 1 to 10 cm;

Table 1
Minimum dose rate per LL obtained considering the whole set of scenarios for each material.

	Aluminum	Concrete	Copper	Inconel	Iron	Steel
Minimum DR/LL (nSv/h/LL)	4,2	6,9	22,5	17,8	12,6	14,6

- Energy of the primary beam particles ranging from 160 MeV to 7 TeV protons;
- Positions in the accelerator (all standard ActiWiz positions and all LHC experiments (Bergstron et al, 1723334; Vincke and Theis, 2014);
- Material composition (Froeschl et al., 2012) for the most typical objects, including aluminum (cf "Aluminum_6060" in (Froeschl et al., 2012)), iron ("pure_IRON"), stainless steel ("Steel_304L"), copper ("Copper_CuOFE"), Inconel ("Inconel-0.21-Co"), concrete and polyethylene ("Polyethylen"). It should be noted that a much larger range of possible values had been considered in a preliminary study, for example to investigate the feasibility to use mass-dependent acceptance criteria. The range presented above is indeed the result of an exhaustive iterative process of optimization with different techniques of data learning, including for example decision trees (Barros et al., 2015). The case of lead was also covered by the preliminary study, which showed that most of the activation scenarios would have a dose rate at LL equal 1 below 5 nSv/h. Hence, lead was excluded from this study. For each metal type (aluminum, iron, stainless steel, copper and Inconel), we determined the activation scenario with the smallest DR/LL. It turned out that aluminium penalizing scenario is the most conservative as it had the lowest DR/LL value (Table 1).

Fig. 1 below shows the results of the factor analysis for aluminum. The purpose of the factor analysis is to reduce the dimensionality of large datasets, to classify and focus only on impacting parameters. It is here used in order to explore correlations between the parameters. The analysis is done by finding the principal components. These components represent linear combinations of the parameters and allow to express information as a new set of parameters. For instance, component 1 is made of width, length of objects and DR/LL (Fig. 1). The DR/LL is represented by component 1 (18.1% of its variation), component 2 (48.4% of its variation) and component 5 (33.4% of its variation). We only focus on these components for the analysis as we are interested by the behavior of DR/LL. The input parameters (also called "variables") are represented by vectors on the unitary circle. The variable denoted V is the length (or width) of the object, W is the thickness, and T_{cool} is the cooling time. The remaining input parameters (e.g. the beam energy or the position in the accelerator) are represented by very short vectors, indicating that their contribution to our factor analysis – and more specifically to DR/LL - can be safely disregarded. They have been here removed from the graph for readability purpose. This graph can be understood as follows:

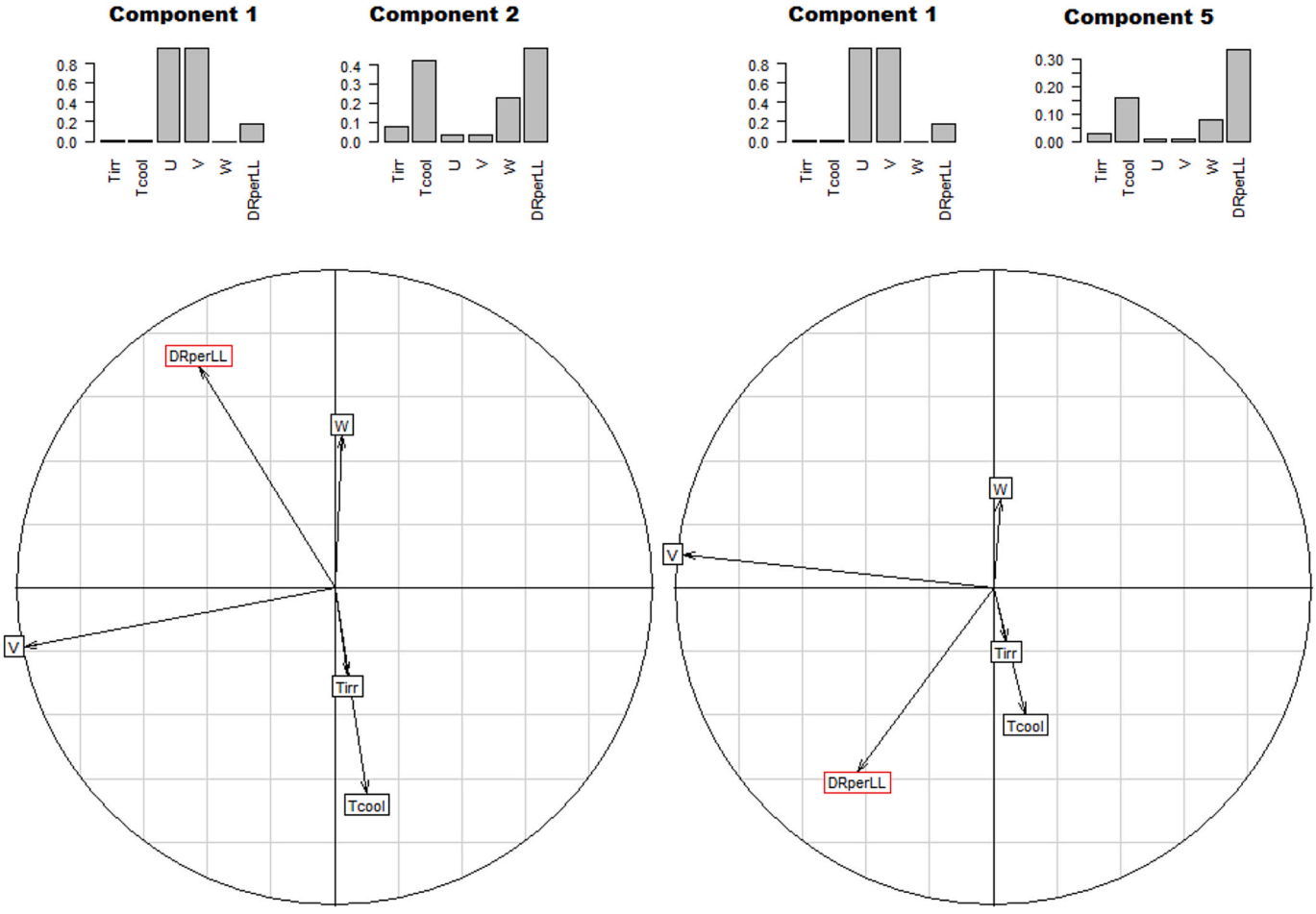

Fig. 1. Factor analysis of mixed data for aluminum. Left figure represents the unitary circle for components 1 and 2 and right figure, the unitary circle for components 1 and 5.99.9% of the DR/LL variability is represented by these two components. Energy and position variables are removed for readability purpose as they do not affect the DR/LL. U and V have a similar behavior and are coupled.

- Vectors which have a length close to 1, are well represented in the space of the two principal components. This is the case for example for DR/LL as well as the U, V dimensions (which are coupled). On the opposite, the irradiation time (T_{irr}) is found to have a relatively short length which can be understood as having a low impact. Indeed, we can see that Tirr and Tcool vectors point in the same directions with a Tirr vector amplitude shorter than the Tcool one (norm below 1). This indicates that the Tirr parameter is not as well represented as Tcool in the components graph. As these components explain 99.9% of the variance of DR/LL, we conclude that Tirr and DR/LL are less correlated than Tcool and DR/LL. This can understand as follows:
  - o Increasing the irradiation time will increase the activity of radionuclide produced, by a scaling process, i.e. with conservation of the radionuclide's activity fractions. Hence, the modification of DR and the modification of LL will be quite similar, having low impact on the ratio.
  - o Increasing the cooling time will trend to modify the activity of radionuclide produced but as well the radionuclide vector due to the decay. Hence, the variation of DR and LL are not similar, leading to a higher spread of the ratio DR/LL
- The correlation of two parameters is represented by the angle between these two vectors. Hence, two vectors with opposite directions are anti correlated. A perturbation of one parameter is linked with an inversely proportional variation of the other. On the opposite, two vectors with same direction are fully correlated. And finally, perpendicular vectors denote quantities that are uncorrelated.

Reading the graph, we observe that U,V are positively correlated with DR/LL. The correlation factor value is 0.23. W is positively correlated with DR/LL on the left graph and negatively correlated on the right graph. However, it has a better representation on the left graph and the correlation factor value is 0.17. Tirr and Tcool are negatively correlated with DR/LL, with a correlation factor, respectively of −0.11 and −0.26 (vector length is shorter for Tirr compared to Tcool). The correlations are calculated using the Pearson's formulae as detailed in Equation (3). As a conclusion, we can increase the DR/LL by increasing the length/width and thickness (these vectors are positively correlated) or by reducing the cooling time (negatively correlated).

$$r_{x,DR/LL} = \frac{\hat{a}_{i=1}^{n}(x_i - x)(DR/LL_i - DR/LL)}{\sqrt{\hat{a}_{i=1}^{n}(x_i - x)}\sqrt{\hat{a}_{i=1}^{n}(DR/LL_i - DR/LL)}} \quad (3)$$

Equation (3). Correlations between a parameter x and the dose rate at LL equal 1.Where: $r_{x,DR/LL}$ represents the correlation between DR/LL (evaluated with ActiWiz) and the parameter x (e.g. Tirr or Tcool), x is the mean of the parameters x_i and n is the number of calculations.

The ranges of input parameters listed at the beginning of this section are optimized in the sense of fulfilling the requirement of DR/LL ≥ 5 nSv/h, for the case of aluminum (as envelope case for other metals), once the minimum length/width is set to 30 cm and the minimum thickness to 5 cm. The input parameters of polyethylene and concrete show similar correlation patterns as for aluminum. However, polyethylene has lower values of DR/LL. In fact, for polyethylene, the gamma dose rate measurement is due to the Be-7 activity produced after irradiation. Since, the Be-7 half-life is 53 days, its corresponding activity decreases fast with increasing cooling times. Hence, the dose rate falls below the detection limits and cannot be measured. This effect induces a strong decrease of the DR/LL with cooling time. Hence, we need to reduce the acceptable range of cooling time from two years down to four months maximum for polyethylene. The result of the factor analysis is given in Table 2. This table provides a preliminary set of acceptance criteria to guarantee that the dose rate value is below 5 nSv/h at 10 cm for an LL value of 1. This set of criteria will be useful for the classification of objects at the exit from the accelerators.

The actual value of DR/LL for a given object, which complies with the criteria in Table 2, will certainly depend on the specific material composition and activation scenario of the object considered. At the same time, the factor analysis shows that the possible values of DR/LL would have a median of 32 nSv/h, with an interquartile range from 18 to 60 nSv/h - which is well above the dose-rate constraint of 5 nSv/h.

Table 2
Preliminary set of acceptance criteria for the use of a dose-rate measurement in view of material classification. Due to the comparably low impact no further restriction on the irradiation time (1 day ≤ T_{irr} ≤ 30 years) is required.

Material	Dimensions	Cooling time
Metals	≥30 × 30 × 5 cm^3	≤2 years
Concrete	≥30 × 30 × 5 cm^3	≤2 years
Polyethylene	≥30 × 30 × 5 cm^3	≤4 months

Table 3
Percentages of cases for which DR/LL can be below 5 nSv/h for the 14 490 retained scenarios with criteria of Table 2.

Material	<5 nSv/h/LL at 10 cm	≥5 nSv/h/LL at 10 cm
Aluminum	0.4% (60/14 490)	99.6% (14 880/14 490)
Concrete	0% (0/14 490)	100% (14 490/14 490)
Copper	0% (0/14 490)	100% (14 490/14 490)
Inconel	0% (0/14 490)	100% (14 490/14 490)
Iron	0% (0/14 490)	100% (14 490/14 490)
Stainless steel	0% (0/14 490)	100% (14 490/14 490)

The factor analysis also suggests that the DR/LL can be below 5 nSv/h for a very limited number of cases (Table 3, 60 scenario over 14 490 for aluminum material lead to a DR/LL below 5 nSv/h/LL). These 60 scenarios concern objects irradiated near the tunnel wall of LINAC4 under very specific irradiation conditions or in areas near the ALICE detector.

It should be noted that the range of parameters has been chosen as very wide, considering also somewhat exotic and rare cases. In order to evaluate the real robustness of the recommended MDDR a statistical analysis has to be carried out, which takes into account the actual occurrence frequency of a given activation scenario based on empirical data. This statistical analysis is the subject of the next section.

We conclude this factor analysis by observing that in the worst-case scenario – i.e. an object classified as non-radioactive and with a dose-rate exactly at the cut-off value of 5 nSv/h - the estimated fraction of LL limit would have a median of 0.16 with an interquartile range from 0.08 to 0.29, and a highest value for the most conservative scenario of LL equal 1.2. These results are shown in Fig. 2. The boxplot on the left describes the distribution of dose rates at LL equal 1 of aluminum objects with dimensions above 30 × 30 × 5 cm^3. We can read on the boxplot that, the minimum dose rate at LL equal 1 would be 4.16, which corresponds to LL equal 1.2 with the MDDR of 5 nSv/h. The histogram on the right shows the distribution of the LL in the case of a dose rate at 5 nSv/h. The red vertical line is the limit of LL = 1.

It should once more be stressed that this most conservative scenario of finding a dose rate value of 5 nSv/h at a radiotoxicity level of LL equal 1.2 occurs due to the fact that a very large range of parameters are being considered. However, Fig. 2 shows that this is an extremely rare case and this analysis does not even include yet the actual frequency of occurrence in practical application, which can only be obtained by doing statistical analysis of empirical data as shown in the next section and the risk study of section 3.

3.2. Statistical analysis

There are 3′531 objects traced in TREC (Kepinski et al, 2013b) at the exit of the accelerators, which were classified as non-radioactive (with respect to LE limits) via a dose-rate measurement in 2017. About 58% of these objects would have met the acceptance criteria given Table 2. These objects are therefore representative of those that would undergo the classification procedure with the 5 nSv/h MDDR – in terms of size

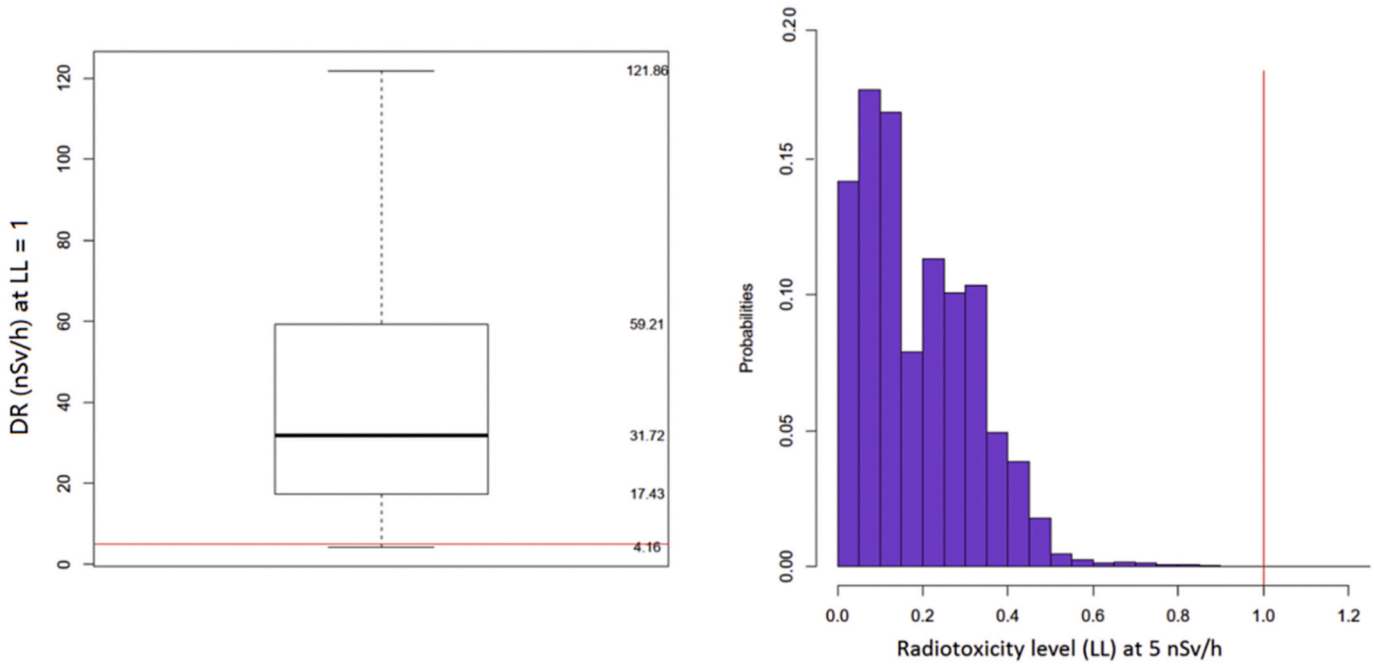

Fig. 2. Distributions of DR/LL (left) and LL fraction of for dose rate of 5 nSv/h at 10 cm (right). Red lines represent the reference values of 5 nSv/h (left) and 1.0 (right). (For interpretation of the references to colour in this figure legend, the reader is referred to the Web version of this article.)

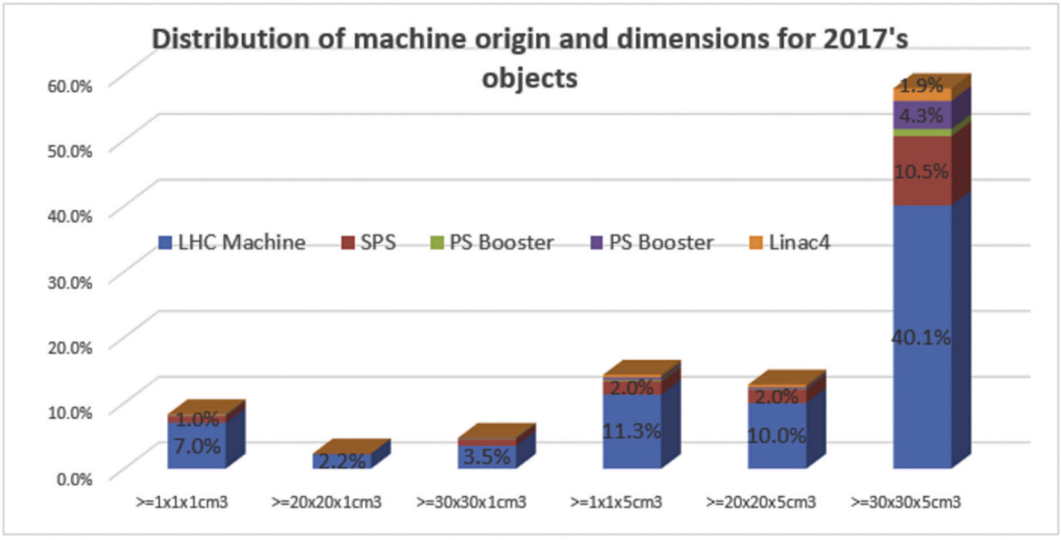

Fig. 3. Statistical distribution of machine of origin and size of non-radioactive objects.

and machine of origin.

As shown in Fig. 3, for each value of possible size and machine of origin we associate a statistical weight that is proportional to the number of instances found in TREC. We therefore assume that if a certain type of object was frequently encountered at the exit of the accelerator in 2017, it is then plausible that similar objects are likely to be encountered in the following years as well.

For the material type, we have applied, in the calculations, the same statistical material distribution found in over 1′000 m^3 of very-low-level radioactive waste for the SHERPA waste elimination campaigns (Zaffora, 2017); Since 2016, CERN characterized around 1000 m^3 of conditioned activated metallic waste. The SHERPA project (SHEaR Process Assessment) aims at the disposal of activated metals in the French final repositories for waste with very-low activity. We assume that such a material distribution is representative of the objects irradiated at CERN facilities: 60% of iron, 20% of stainless steel and 20% of aluminum.

Regarding the remaining input parameters (e.g. the irradiation time), we have applied a uniform probability distribution to reflect our current state of knowledge and to avoid introducing any unjustified bias.

Because of the fine granularity of possible values of input parameters and in order to properly account for their statistical probability, over 2.3 million calculations were performed for each type of material considered. The total set of results originates from 11 million calculations of dose rates and LL to statistically represent the DR/LL of objects found at the exit of the accelerator machines according to their physical characteristics (cooling time, irradiation time, material, location in accelerator, primary particle energy, size).

Fig. 4 shows the distribution of DR/LL, taking into account the experimental probability distribution of the different input parameters.

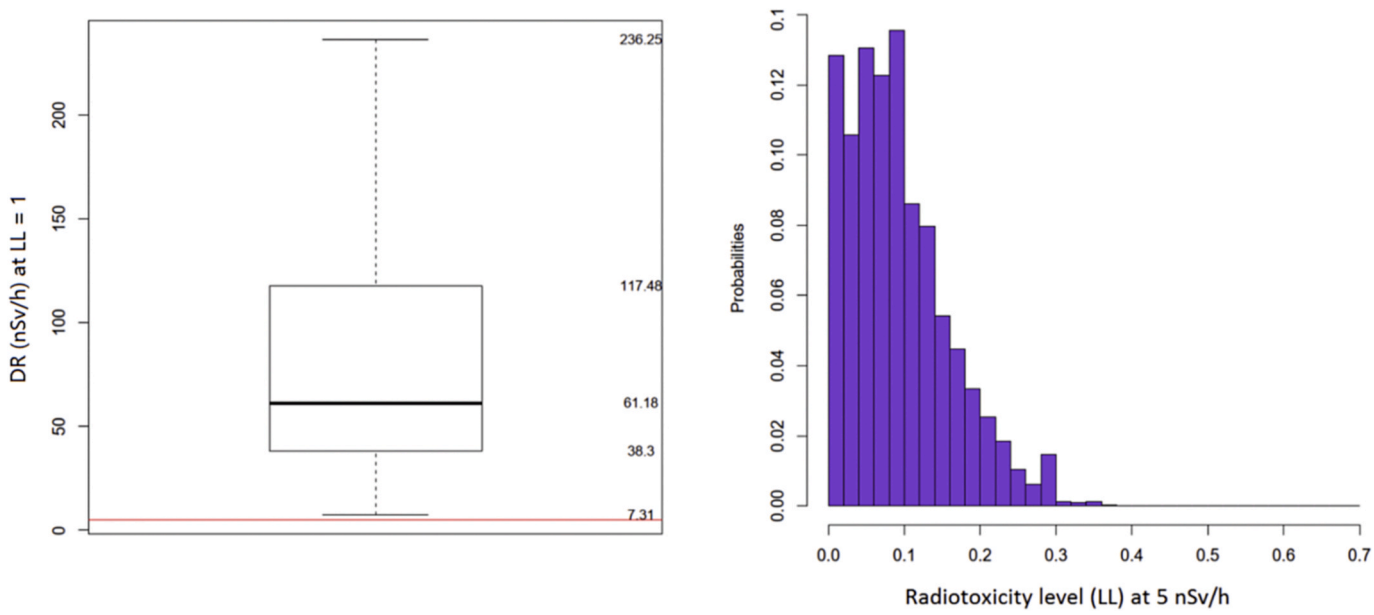

Fig. 4. Distributions of DR/LL and of fraction of LL for objects measured in 2017 and meeting the acceptance criteria.

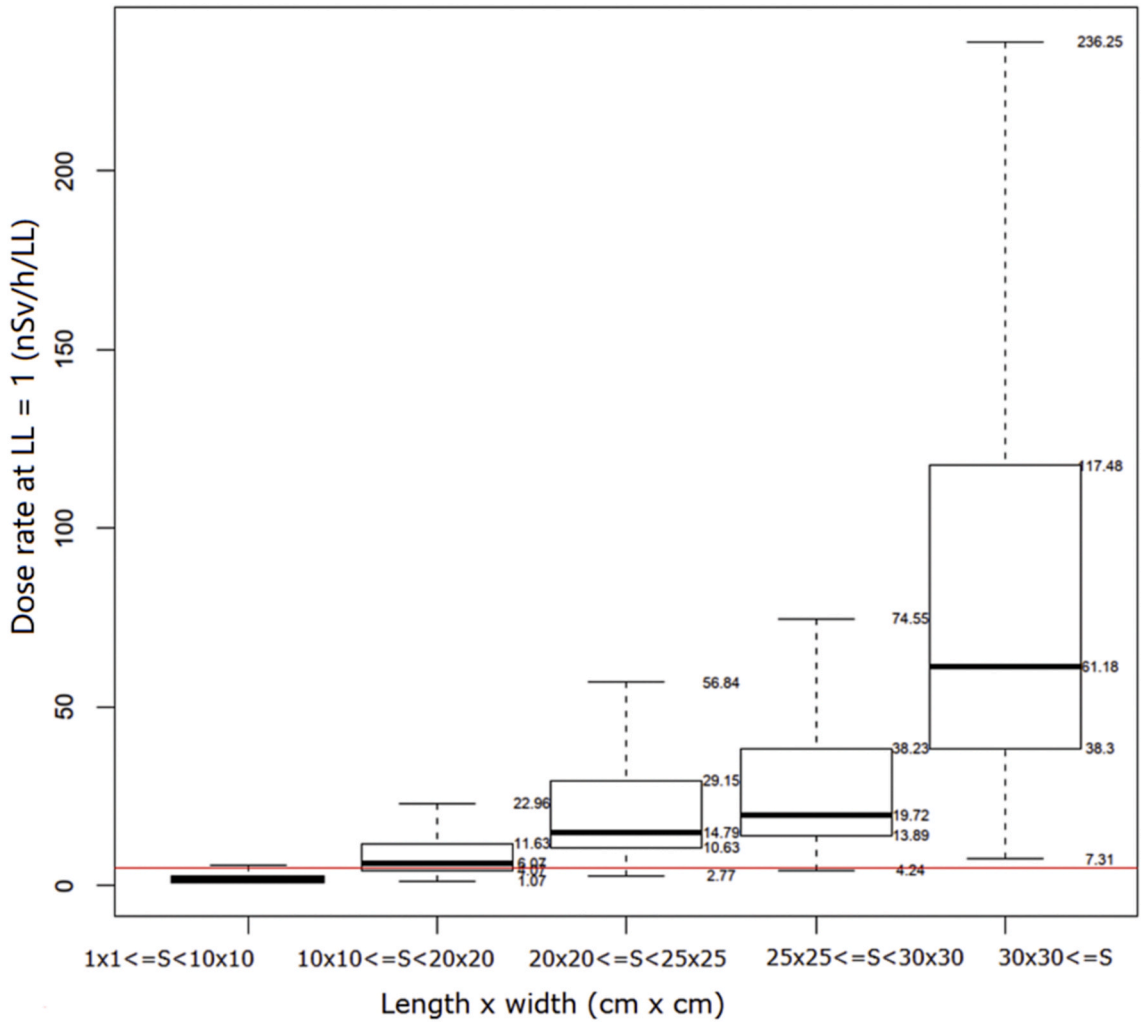

Fig. 5. Distributions of DR/LL depending on the measured length x width for TREC 2017's metallic objects with a thickness $\geq$ 5 cm.

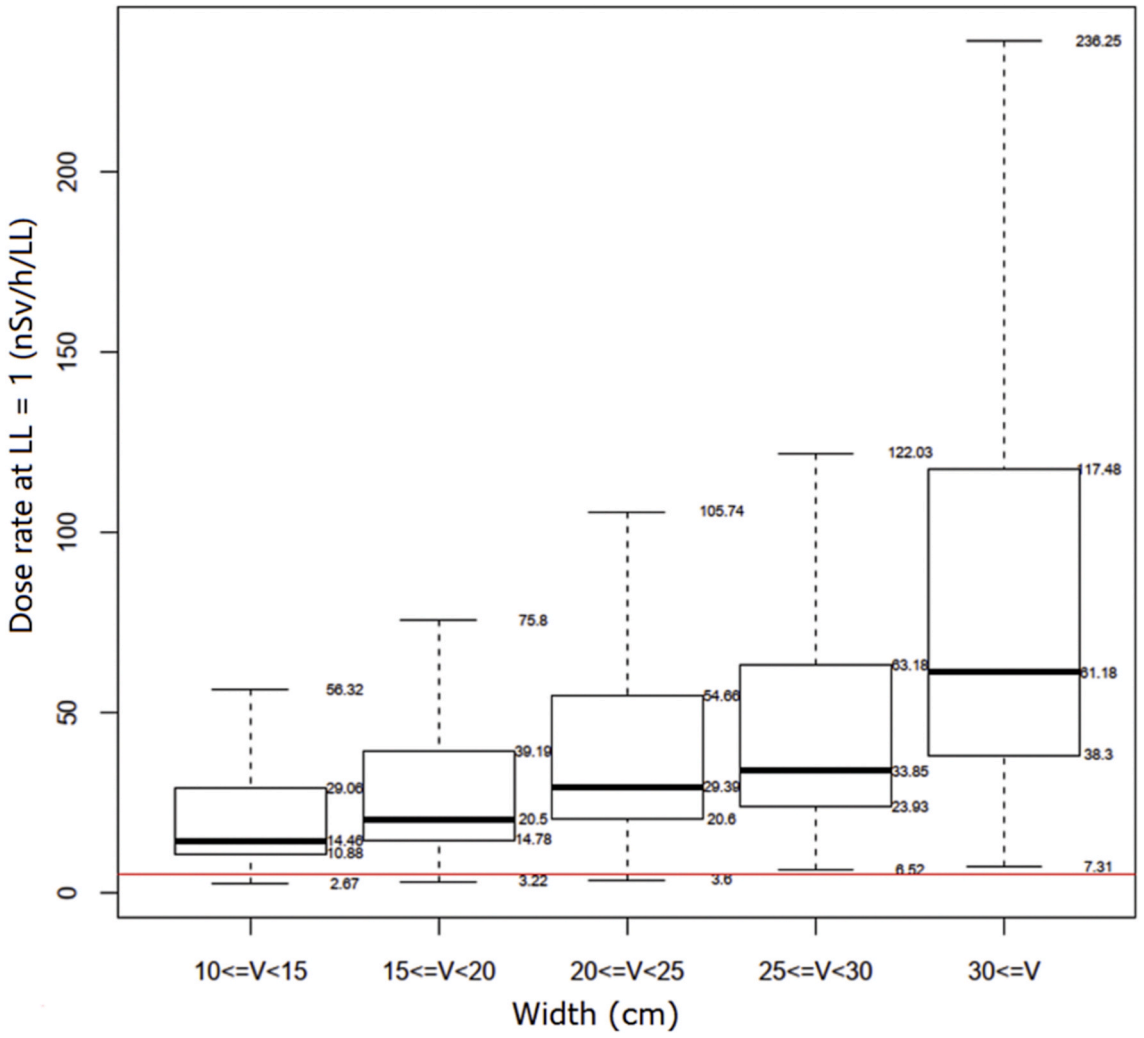

Fig. 6. Distributions of DR/LL depending on the measured width for TREC 2017's metallic objects with a thickness ≥5 cm and a length ≥ 30 cm.

The median DR/LL of the data set is 61 nSv/h with an interquartile range from 38 to 118 nSv/h. These values are significantly higher than the theoretical range found in section 2.1, where all activation scenarios were hypothetically considered to occur with the same probability due to the lack of better knowledge. Moreover, the lowest value of DR/LL is 7 nSv/h, which is above MDDR of 5 nSv/h. This result suggests that the MDDR of 5 nSv/h would have allowed for the correct identification of every radioactive object measured in 2017, leading to a reliability level of better than 1 in 3′531 (i.e., >99.99%). Nevertheless, we recommend that quality controls are regularly performed in the years to come in order to identify any new trend in the properties of objects at the exit from accelerators, and to assess their impact on the MDDR.

It should be noted that in addition to their reliability, the acceptance criteria defined in Table 2 are optimized in the sense that they would have covered the majority (over 58%) of objects measured in 2017.

4. Risk analysis

A risk analysis was performed to evaluate the possible impact of uncertainties or errors on the material classification. In particular, the analysis is based on the statistical distributions presented in section 2.2.

4.1. Measurement uncertainty

Under the conditions defined in section 2, the uncertainty U on the net count rate can be calculated with Equation (4) from ISO11929-1 (ISO11929), where $k_{1-\gamma}$ is the quantile of the standard normal distribution for a given confidence level (set at 97.5% for the present study), and t_0 and t_s are the background and sampling counting times.

$$U = \left(k_{1-(\gamma/2)}\right)\sqrt{\frac{R_0}{t_0}+\frac{R_s}{t_s}} \quad (4)$$

Equation (4). Uncertainty of the dose-rate measurement.

4.2. Impact of the variation of lateral dimensions

According to the acceptance criteria given in Table 2, objects with surfaces smaller than 30 × 30 cm^2 shall be excluded. Fig. 5 shows the impact on DR/LL of an error in measuring the surface. An error of 33% of the assumed surface due to simultaneous mistakes on each of its dimensions (i.e. 30 × 30 cm^2 assumed for an object measuring 26 × 26 cm^2 in reality) would not lead to any classification mistake with respect to the objects measured in 2017 as the DR/LL remains above 5 nSv/h/LL. We note in passing that this analysis restricts itself to mistakes in both dimensions as overly gross mistakes in one dimension (e.g. 10 × 90 cm^2 which would still lead to a surface of 900 cm^2 but grossly violate the requirement of ≥30 cm per dimension) can be ruled out as highly improbable.

Failure to apply the sorting criterion of dimensions – for example by accepting objects with a length d of $20 \leq d \leq 30$ cm in each dimension, which reflects a deviation of up to more than 50% of the required surface – would still lead to correct material classification in 99.99% of the cases

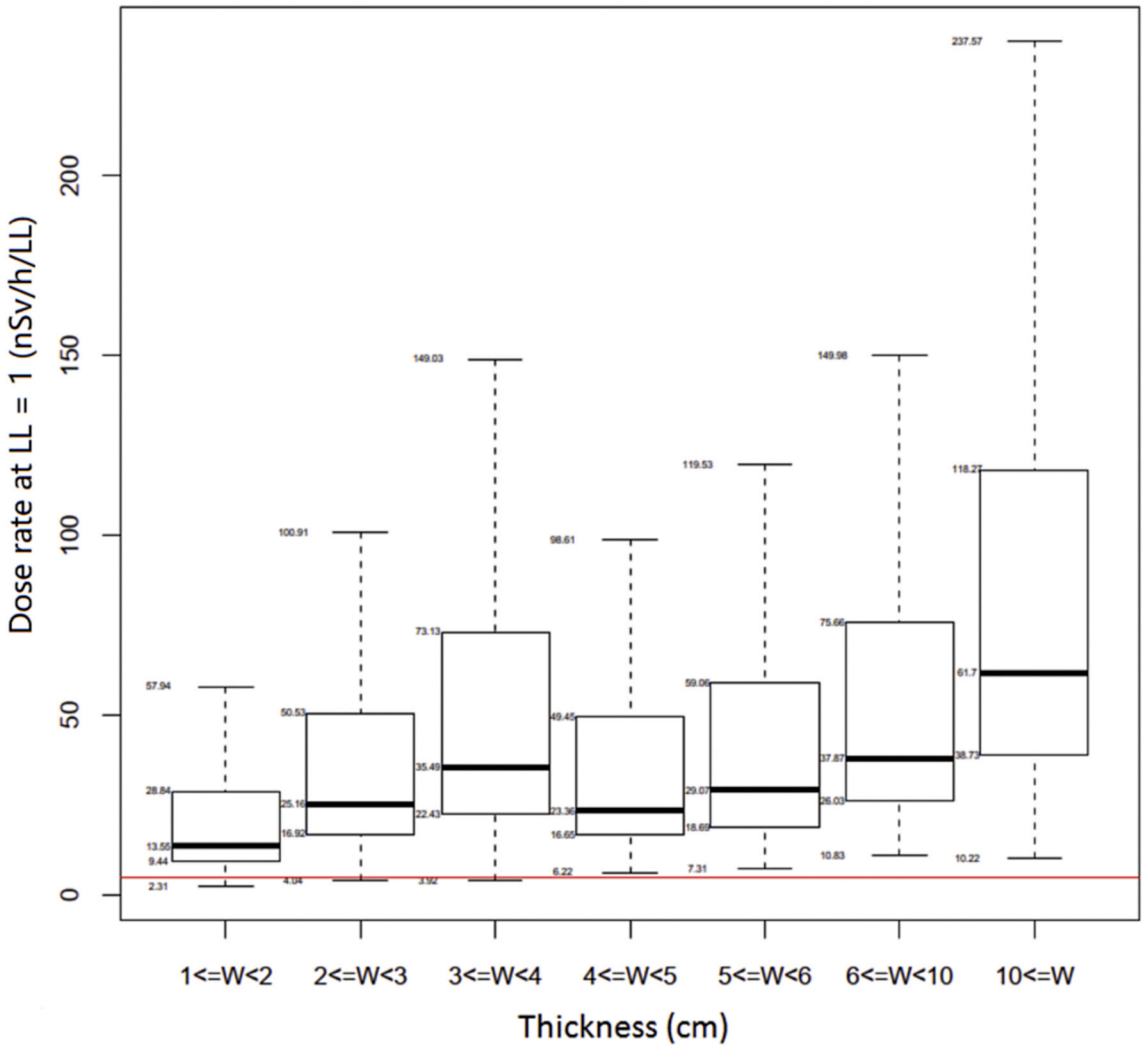

Fig. 7. Distributions of DR/LL for TREC 2017's metallic objects with a surface above 30 × 30 cm^2.

with a maximum value of LL of 1.8. Indeed, only 0.01% of objects would have a DR/LL below 5 nSv/h/LL.

In addition, the risk of a mistake in one dimension of the surface has been studied. Fig. 6 shows the impact on DR/LL of erroneously measuring the width. An error of 33% of the width (i.e. 30 cm assumed for an object with a real width of 22.5 cm) would not lead to any classification mistake with respect to the objects measured in 2017.

Failure to apply the sorting criterion of dimension – for example by accepting objects with width as low as 20 cm – would still lead to correct material classification in 99.99% of the cases with a maximum value of LL of 1.4.

4.3. Impact of varying thickness and hollow objects

According to the acceptance criteria given in Table 2, objects with thicknesses smaller than 5 cm shall be excluded. Fig. 7 shows the impact on DR/LL of a mistake in measuring the thickness. An error of 25% in thickness (i.e. 5 cm measured for a 4 cm object) would not lead to any classification mistake with respect to the objects measured in 2017.

Failure to apply the sorting criterion of thickness – for example by accepting objects with thickness from 1 to 5 cm – would still lead to correct material classification in 99% of the cases.

A mistake in the measurement of the thickness can also be regarded as a case of mismatch between theoretical density (e.g., density of bulky materials – as assumed in this study) and apparent density (e.g., density of materials with voids). Experience with radioactive waste suggests that such a mismatch can be as high as a factor of 5 for typical cases, which is comparable with the mistake introduced by accepting objects of thickness of 1 cm when the limit is set at 5 cm.

Fig. 8 shows the DR/LL for objects measured in 2017 and with thicknesses larger than 1 cm, as a function of their mass (i.e., with less or more than 10 kg). Although the overall success probability for the classification is 99%, in the specific case of objects heavier than 10 kg the success rate is better than 99.99%. More specifically, the median is 60 nSv/h with an interquartile range from 37 to 115 nSv/h, and 1st percentile at 15.4 nSv/h. We therefore recommend that a compensatory measure is introduced in terms of minimum mass, to compensate for cases of hollow objects with small apparent density.

4.4. Mixtures of materials

Metallic objects can be made of one single metal type that might contain impurities, or as an assembly of different metal types that are heterogeneously distributed. As demonstrated in section 2.1, the case of an assembly of different types of metals is fully covered by the case of an object made of aluminum, which is more conservative than any of the other metals considered. For sake of simplicity, we consider only the case of objects coming from the LHC – which represent the majority of the cases of interest. Nevertheless, the study was extended to cover 86 possible chemical compositions, leading to over 50′000 activation

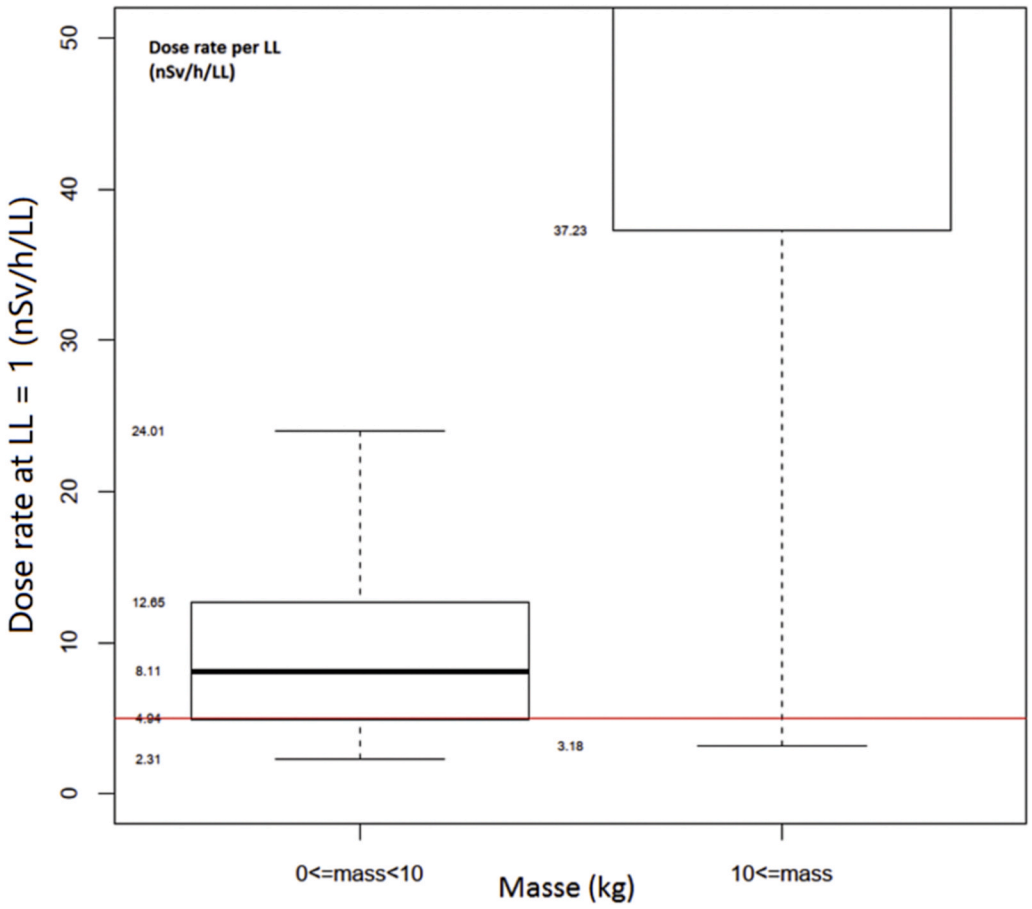

Fig. 8. Distributions of DR/LL for objects measured in 2017, depending on mass of the objects.

Table 4
Composition of Aluminum_6060 (mass fraction).

ALUMINUM	COPPER	CHROMIUM	IRON	MAGNESIUM	MANGANESE	SILICON	TITANIUM	ZINC
98.375	0.1	0.05	0.2	0.475	0.1	0.45	0.1	0.15

scenarios.

A study based on results from paragraph 2.2 has been performed to quantify the risk in case of encountering a mixture of 99%, 95%, 90%, 80% and 70% Aluminum_6060 (composition in Table 4) and 1%, 5%, 10%, 20% and 30% of the 80 stable elements found in the periodic system that can be assumed to occur as impurity. For this study, 2 million calculations have been carried out. This study focused on statistical data as this is in practice the predominant origin of material to be classified, as can be seen in the results presented in Fig. 9. The worst case is Zinc mixed with Alumnium_6060.

The only elements which could have a detectable impact on the distribution of DR/LL while mixed aluminum are Cd, Li, Tl and Zn.

The dashed curves in Fig. 9 represent the maximum LL reached using these data with different mixture compositions which ratio is read on abscise axis and value on right axis. The percentage of cases from 2017 TREC data which would have been wrongly classified is expressed on the right axis. In summary the conclusions are the following:

- A mixture of 1% of Zinc with 99% of Aluminum_6060 would lead to a maximum LL of 1.12 and a wrong classification of 0.03% of cases from 2017. We observe an asymptotic behavior with the LL of this mixture when ratio of Zinc increases as, at 30% of Zinc, the maximum LL reaches 1.3 (green dashed curves). However, the quantity of wrongly characterized objects remains very low with only 0.37% of errors.
- For Thallium and Lithium, behaviors in terms of maximum LL are similar. For a mixture of 1% of these elements with aluminum we do not exceed LL equal 1. However, the situation changes rapidly with increasing percentage of Thallium in aluminum, as the LL reaches 6.5 at 10% and 24 at 30%. Along with the LL, also the number of cases which suffer from wrong classification increases dramatically. For Thallium and Lithium, we get respectively 3.4% and 1.1% of incorrect characterizations with a mixture of 10% of these elements and respectively 9.7% and 6.6% for mixtures with 30% of these elements.
- Regarding Cadmium mixtures, the maximum LL reached with 1% of this element is below LL equal 1 but increases from 2.2 at a content level of 10% to 6.5 at 30%. However the percentages of cases with wrong characterization remains low and reaches 0.047% with 10% of Cadmium in aluminum_6060 and 0.82% for a mixture with 30% of Cadmium.

It should be noted that for lithium, cadmium and thallium up to 1% in mass, the classification procedure would be successful for every object measured in 2017. We can therefore conclude that the procedure is safe as long as these elements are only present in the form of trace elements,

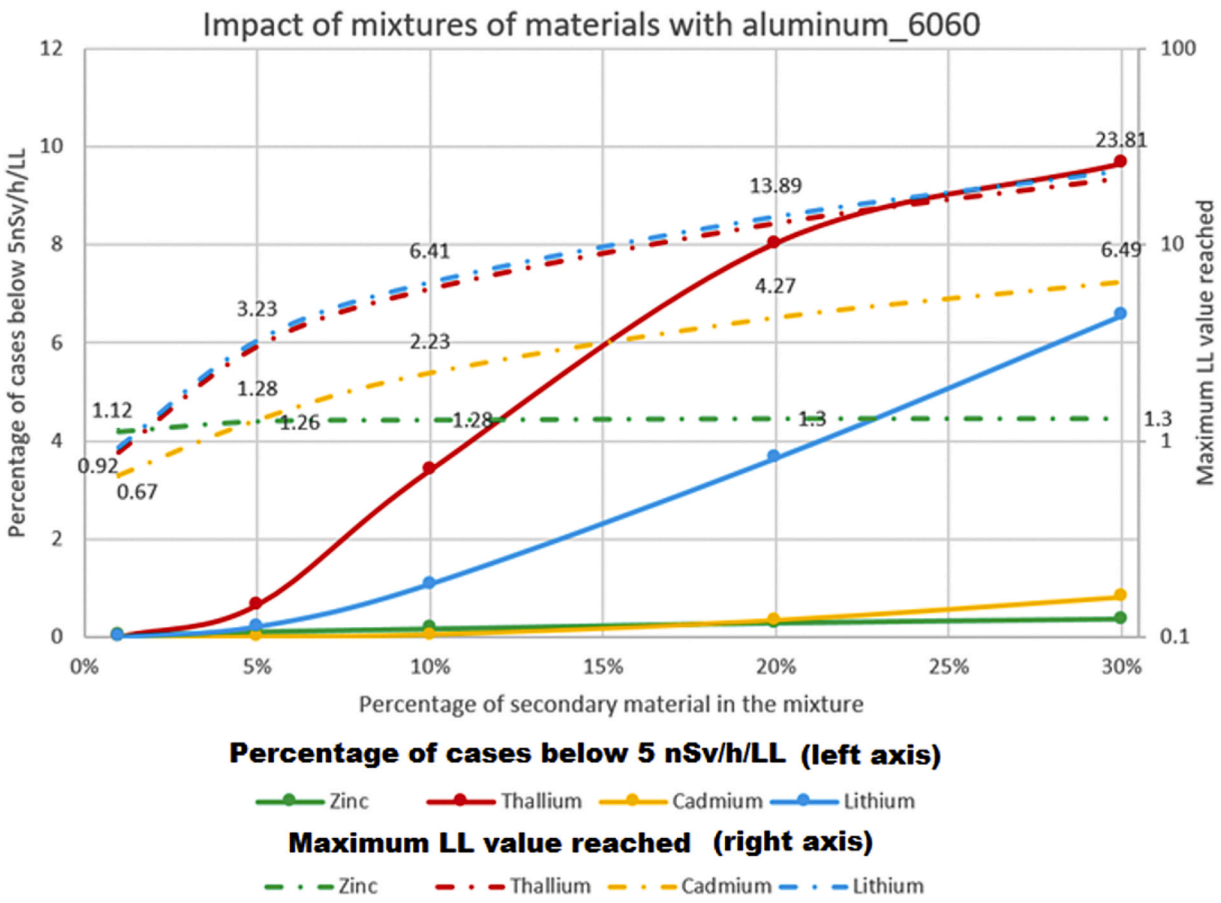

Fig. 9. Maximum LL and percentage of cases which would be wrongly characterized due to mixtures containing 1%, 5%, 10%, 20%, 30% of a potentially problematic material measured together with Aluminum_6060. In accordance with previous studies the scenarios of the statistical study (paragraph 2.2, for aluminum only) have been used as they present the dominant origin of material that is to be classified. Dashed lines present the maximum LL reached and are referenced on the right axis. Straight lines present the percentages of cases below 5 nSv/h/LL and can be read on the left axis. Numbers embedded in the graph correspond to the curve value at 1%, 5%, 10%, 20%, 30%, as can be read on the right axis (Maximum LL value reached).

and if we exclude e.g. Lithium batteries from the objects to be classified.

For zinc, which can be present in galvanized steel, the classification procedure would be successful in more than 99.8% of objects measured in 2017 for a mass fraction of 5% of zinc in aluminum. This result is satisfactory, considering that the typical amount of Zn in galvanized steel is often less than 5% and that aluminum is penalizing compared to steel as demonstrated in section 3.1. We consider it is very unlikely that one object coming from the accelerator can contain components made of pure zinc, and can therefore conclude that these results confirm the robustness of the classification procedure. The pure zinc is then excluded from the current study. Hence, pure zinc will not be handled at CERN for classification purpose. Moreover, the statistics provided by the treatability system at CERN did not reveal such a need for pure zinc classification.

5. Experimental verification

In order to verify experimentally the validity of the MDDR represented within this paper, an activation experiment in the CHARM facility at CERN has been carried out.

In particular, we irradiated two samples which respect the acceptance criteria of Table 2 in order to reach the critical fraction of LL equal 1, and compared the corresponding DR/LL and the respective radionuclide inventories with our analytical predictions.

5.1. Experimental setup

The irradiation took place in CERN's CHARM facility in the East Experimental Area of the Proton Synchrotron (PS), where a 24 GeV/c proton beam impacts on a target, leading to the creation of secondary particles. The characteristics of the proton beam are well known and the quantity of protons impinging on the target is stored in a database that is continuously updated.

Two plates with a size at the lower limit of the acceptance criteria ($30 \times 30 \times 5$ cm^3) and two cubes, made of aluminum and iron, were positioned adjacent to the target where the proton beam impacts (Fig. 10 – "inside wall locations" and Fig. 11).

The fluence of secondary particles at the location of irradiation has been simulated with FLUKA2011.2c.3 (Böhlen et al., 2014; Ferrari et al., 2005; Froeschl et al., 2018a, 2018b). These data in combination with the beam intensity have then been used in ActiWiz Creator to calculate the respective nuclide inventories as a function of the irradiation and cooling times. Therefore, considering the beam intensity (around 3.5E+10 protons per second) and the secondary particle fluence the following irradiation pattern has been applied:

- The Aluminum sample was irradiated for three days and 2 h. One measurement was done after two days of irradiation to ensure that predictions are correct (from 1:23 p.m. on 09/12/2018 to 4:05PM on 09/15/2018);
- The Iron sample was irradiated for 4 h and half (from 9:40AM to 2:06PM on 09/14/2018).

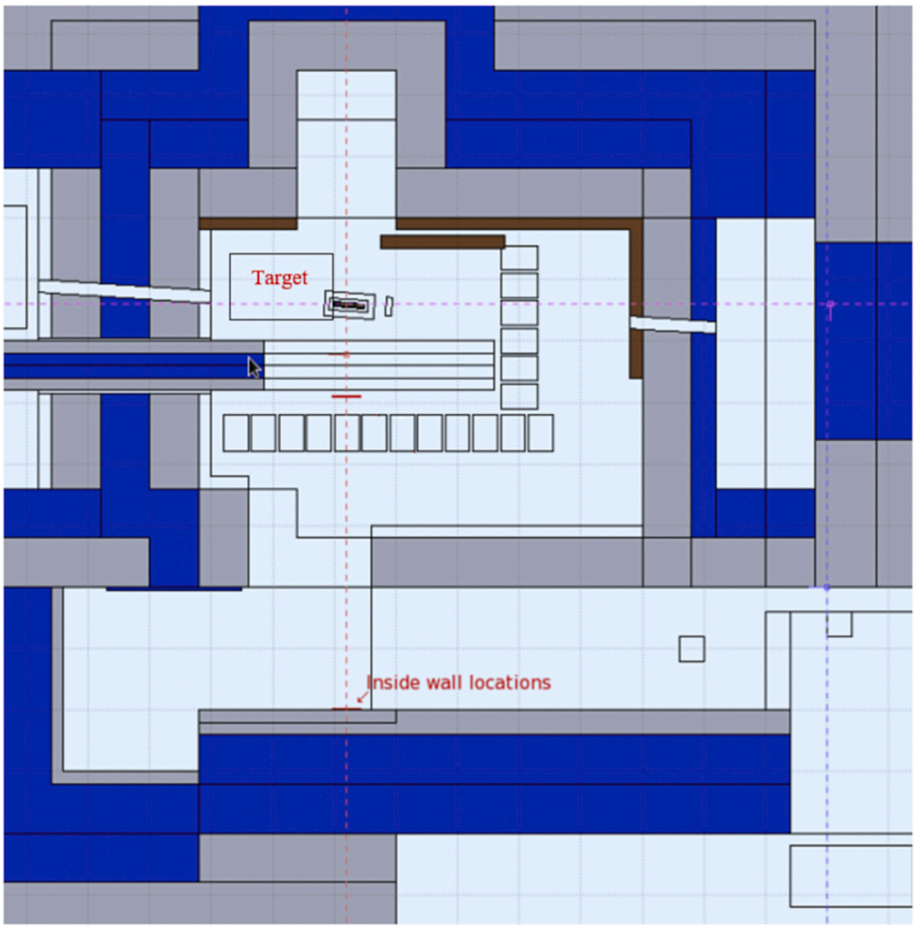

Fig. 10. Section of the FLUKA geometry of the CHARM facility, including also an indication of the irradiation locations. The irradiated objects were located at the position labelled "inside wall locations".

Fig. 11. Samples of Aluminum and Iron irradiated at CHARM.

5.2. Experimental results

Gamma spectrometry measurements were performed after the irradiation to measure the specific activity and assess the corresponding fraction of LL due to gamma emitters.

Table 5 shows the comparison of experimental and calculated activity levels – feeding ActiWiz with fluence spectra –, one week after the end of irradiation. In general, the values predicted by the ActiWiz calculation show good agreement with the measurements, in particular for the main contributors to the dose rate per LL. Observed discrepancies remain below a factor of 2 for radionuclides that have negligible contributions to the LL value (such as Be-7 with LL of 10 and Fe-59 with LL of 1). Moreover, for these radionuclides, the calculation is penalizing.

Dose rate measurements were carried out on the two plates with a BGO detector[2] and – for the sake of comparison - an AD-b dose rate meter[3] over the course of 1 month after irradiation. The lowest dose rate measured when the fraction of LL was 1.0 is 12 nSv/h at 10 cm (Table 6), which is well above the MDDR of 5 nSv/h and the detection limits of both devices. The recommended classification procedure would have therefore succeeded in identifying these two objects as radioactive.

The moment for which LL equal 1 (respectively 7 days and 7 h after irradiation and 33 days and 19 h after irradiation, for the Iron and Aluminum samples) has been determined by decay calculation taking into account the activities and isotopes measured by gamma-spectrometry.

The measurements at 10 cm presented in Table 6 also confirm the very good agreement between the BGO and dose rate measurements with 1 count/s equivalent to 1 nSv/h.

[2] BGO s/n 00104 calibrated on 08/08/2018.

[3] AD-b s/n 161633 calibrated on 20/08/2018; https://www.automess.de/Download/Prospekt_ADb_E.pdf.

Table 5
Comparison of calculations/measurements of specific activities of samples after their irradiation in CHARM. Only the radionuclides contributing to more than 99% of the LL and dose-rate are presented.

1 week after irradiation							
21/09/2018				22/09/2018			
Iron plate				Aluminum plate			
RN	**Act. Exp (Bq/g)**	**Act. Cal (Bq/g)**	**Ratio cal/exp**	**RN**	**Act. Exp (Bq/g)**	**Act. Cal (Bq/g)**	**Ratio exp/cal**
Sc-44	1.11E-02	1.37E-02	1.23	**Be-7**	4.51E-02	1.58E-01	3.50
Sc-46	3.71E-03	4.42E-03	1.19	**Na-22**	5.73E-02	5.65E-02	0.99
V-48	4.77E-02	8.56E-02	1.79	**Na-24**	1.47E-01	1.49E-01	1.01
Cr-51	1.86E-01	2.48E-01	1.33	**Sc-46**	3.66E-03	4.64E-03	1.27
Mn - 52	1.32E-01	1.69E-01	1.28	**Sc-48**	2.94E-03	3.79E-03	1.29
Mn - 54	7.03E-02	7.57E-02	1.08	**V-48**	1.22E-02	2.48E-02	2.03
Co-56	1.96E-03	4.18E-03	2.13	**Cr-51**	5.28E-01	1.23E+00	2.33
Fe-59	2.79E-02	1.00E-01	3.58	**Mn - 52**	2.56E-02	2.53E-02	0.99
LL	**0.97**	**1.2**	**1.24**	**Mn - 54**	2.27E-02	2.75E-02	1.21
				Zn-65	1.77E-02	7.84E-03	0.44
				LL	**1.2**	**1.2**	**1.00**

Table 6
BGO and ADb measurements at LL equal 1 as measured by gamma-spectrometry. Uncertainties provided at 1σ.

	BGO measurement (count/s)		ADb measurement (nSv/h)	
	@10 cm for LL = 1	@contact for LL = 1	@10 cm for LL = 1	@contact for LL = 1
Aluminum plate	12 (5.2%)	24 (3.7%)	12 (11.3%)	30 (10.5%)
Iron plate	94 (1.8%)	170 (1.4%)	91 (10.2%)	151 (10.1%)

Last but not least, this experiment suggests that when we replace a measurement at 10 cm with a measurement at contact, we introduce a safety factor of 2 (gamma attenuation follows an exponential law).

6. Conclusions

Following the introduction of new clearance limits (LL), the classification of material at the exit from the accelerators can still be performed on the basis of a dose rate measurement, by using a FHZ 512 BGO detector. In particular:

- If the measured dose rate is below or equal 5 nSv/h, we can conclude that the object is not radioactive;
- If the measured dose rate is above 5 nSv/h, we cannot exclude that the object is radioactive.

This classification procedure applies to objects which respect the following acceptance criteria:

- Dimensions: $\geq 30 \times 30 \times 5$ cm^3
- Materials: metals except Lead. Concrete and organic compounds are also accepted.
- Equipment containing components with pure Thallium, Lithium or Cadmium shall be excluded (e.g. batteries)
- Mass: $\geq$ 10 kg ($\geq$4 kg in the case of organic compounds)
- Cooling time: $\leq$ 2 years ($\leq$4 months in the case of organic compounds)
- Background level: $\leq$ 35 count/s with FHZ 512 BGO

The maximum LL reached with these criteria is 0.7, which is below the legal limit of 1.0. The typical risks (measurement uncertainty, thickness of the objects, hollow objects, mixture of material) will not affect the success rate of the classification if the above acceptance criteria are met.

Objects which fail to meet the above acceptance criteria, would need complementary measurements or additional calculations using specific scenario parameters that are adapted to the respective situation, in order to be correctly classified via residual dose rate evaluation. For objects that do not comply with the criteria of this study, another dedicated method is developed and described in (Frosio, Menaa, Dumont, Aberle).

Author contribution

The authors do not want to provide a contribution section.

Declaration of competing interest

The authors declare that they have no known competing financial interests or personal relationships that could have appeared to influence the work reported in this paper.

Acknowledgements

The authors would like to thank Doris Forkel-Wirth as well as Reiner Geyer for the fruitful discussions and feedback.

References

Barros, R.C., F De Carvalho, A.C.P.L., Freitas, A.A., 2015. Automatic Design of Decision Tree Induction Algorithms, ISBN 978-3-319-14230-2.

I. Bergstrom et al., FLUKA Estimated Particle Fluence in the Four Major LHC Experiments for Actiwiz3. CERN EDMS 1723334.

Böhlen, T.T., Cerutti, F., Chin, M.P.W., Fassò, A., Ferrari, A., Ortega, P.G., Mairani, A., Sala, P.R., Smirnov, G., Vlachoudis, V., 2014. The FLUKA code: developments and challenges for high energy and medical applications. Nucl. Data Sheets 120, 211–214.

Determination of the Detection Limit and Decision Threshold for Ionizing Radiation Measurements, Part 1: Fundamentals and Application to Counting Measurements without the Influence of Sample Treatment, ISO11929-1.

A. Ferrari, P.R. Sala, A. Fasso`, and J. Ranft Fluka: A Multi-Particle Transport Code. CERN-2005-10 (2005), INFN/TC_05/11, SLAC-R-773.

R. Froeschl, C. Theis, F. La Torre, H. Vincke, N. Walter, S. Sgobba. Radiological Hazard Classification of Material in CERN's Accelerators. ERN-DGS-2012-003-RP-IR, EDMS. ID: 1184236, Geneva.

Froeschl, R., Iliopoulou, E., Brugger, M., Roesler, S., Malacrida, F., Lazzaroni, M., Lendaro, J., 2018a. Radiation Protection Aspects of the Commissioning and Operation of the CERN High Energy Accelerator Mixed Field (CHARM) Facility in the CERN East Experimental Area. SATIF-13, NEA/NSC/R(2018)2, pp. 163–171.

Froeschl, R., Brugger, M., Roesler, S., 2018b. The CERN High Energy Accelerator Mixed Field (CHARM) Facility in the CERN PS East Experimental Area. In: Shielding Aspects of Accelerators, Target and Irradiation Facilities - SATIF 12 Workshop, Proceedings in NEA/NSC/R(2018)2, pp. 163–171.

Frosio, T., Menaa, N., Dumont, G., Aberle, F., March 2020. New methodology for in-situ classification of radiological items with a clearance monitor system. Nucl. Instrum. Methods 966.

I. T. Jolliffe, J Cadima. Principal component analysis: a review and recent developments. Phil. Trans. R. Soc. A 374: 20150202.

M.P. Kepinski et al.. TREC: traceability OF radioactive equipment at cern. Proceedings of IPAC2013, (Shanghai, China).

M.P. Kepinski et al.. TREC: Traceability of Radioactive Equipment at CERN. Proceeding of IPAC2013. Shangai, China. ISBN 978-3-95450-122-9.
Klumpp, J., Miller, G., Poudel, D., June 2018. A new approach to counting measurements: addressing the problems with ISO-11929. Nuclear Instrum. Methods: A 892.
N. Neff. Determination of Operational Parameters of a Scintillator-Based Radiation Measurement Detector. CERN EDMS 823821.
Ordonnance sur la radioprotection ORAP, 2018.
Pagès, J., 2014. Multiple Factor Analysis by Example Using R, ISBN 9781482205480.
C. Theis, H. Vincke, Development of a Residual Dose Rate Module for ActiWiz 3.3.
Vincke, H., Theis, C., 2018. ActiWiz 3 – an overview of the latest developments and their application. IOP Conf. Ser.: J. Phys. Conf. 1046.
Vincke, Helmut, Theis, Christian, 2014. ActiWiz – optimizing your nuclide inventory at proton accelerators with a computer code. In: Proceedings of the ICRS12 conference, 2012, 4. Progress in Nuclear Science and Technology, Nara, Japan, pp. 228–232.
Walter, N., 18th of November 2015. Development of an In-Situ Radiological Classification Technique for Material from CERN's Accelerator Facilities. PhD Tech. U.
Wold, S., Esbensen, K., Geladi, P., 1987. Principal component analysis. Chemometr. Intell. Lab. Syst. 2, 37–52.
Zaffora, B., 2017/9/8. Statistical Analysis for the Radiological Characterization of Radioactive Waste in Particle Accelerators. PhD thesis Conservatoire national des arts et métiers - CNAM.